Superconducting energy gap from break-junction tunneling spectroscopy in the ternary silicide CaAlSi

S. Kuroiwa,[1] T. Takasaki,[2] T. Ekino,[2] and J. Akimitsu[1]
[1]*Department of Physics and Mathematics, Aoyama-Gakuin University, Fuchinobe 5-10-1, Sagamihara, Kanagawa 229-8558, Japan*
[2]*Graduate School of Integrated Arts and Sciences, Hiroshima University, Kagamiyama 1-7-1, Higashi-Hiroshima, Hiroshima 739-8521, Japan*

(Received 11 March 2007; revised manuscript received 3 August 2007; published 12 September 2007)

Tunneling spectroscopy using a break-junction technique has been conducted to determine the superconducting gap structure of the ternary silicide-layered superconductor CaAlSi with and without superstructure. We find that the tunneling conductance in CaAlSi shows a single gap feature, which can be described by the BCS density of states. The gap size Δ obtained from the tunneling conductance in CaAlSi without superstructure is estimated to be approximately 1.0 meV, corresponding to a weak-coupling gap ratio. On the other hand, for a specimen with superstructure, the largest gap, $\Delta=1.5$ meV, significantly deviates from the BCS value, indicating strong-coupling superconductivity. These results demonstrate systematic variations in the pairing interaction with superstructure formations, which are consistent with heat capacity measurements.

DOI: 10.1103/PhysRevB.76.104508 PACS number(s): 74.50.+r, 74.70.Ad, 74.25.Jb

I. INTRODUCTION

The discovery of superconductivity in MgB_2 with the layered AlB_2-type structure[1] has refocused interest onto related compounds as a possible basis for developing new superconductors. In particular, an interesting class of material is the ternary silicide superconductor, such as M_1M_2Si (M_1: Ca, Sr, Ba and M_2: Al, Ga) which also has the AlB_2-type crystal structure with the honeycomb layer formed by M_2 and Si atoms.[2–4] Since M_1M_2Si has a practical advantage over MgB_2 that large single crystals are available, it has been stimulating active investigation as a reference material of MgB_2.

According to a recent report,[5] CaAlSi (CAS) exhibits two types of multistacked crystal structure that indicates a clear fivefold (5*H*-CAS, $T_c\sim5.7$ K) or sixfold (6*H*-CAS, $T_c\sim7.8$ K) superlattice along the *c* axis caused by buckling and rotation in the AlSi layer. It is notable that the differences between the two types of multistacked structures are attributed to the 60° rotation of the Al/Si arrangement in the AlSi layers around the *c* axis, and the buckling and flat AlSi layers in different sequences in the two structures (see Fig. 1). On the other hand, we have reported on clean CAS, which has only a flat AlSi layer with Al and Si atoms being distributed regularly in the hexagonal (B_2) plane without a superstructure (1*H*-CAS, $T_c\sim6.5$ K).[6] Interestingly, we have found that T_c and many other transport properties in CaAlSi depend on the superstructure periodicity.[6] For instance, the field-induced magnetic response in 1*H*-CAS exhibits almost isotropic characteristics for each crystal axis, while that in superstructured specimens (5*H*- and 6*H*-CAS) shows anisotropic ones. Moreover, in our previous heat capacity measurements, the sizes of the superconducting gap in 5*H*- and 6*H*-CAS were far larger than that expected for the BCS weak-coupling limit (i.e., $2\Delta/k_BT_c$: 6*H*-CAS$\sim$5.2 and 5*H*-CAS$\sim$4.4). On the other hand, the $2\Delta/k_BT_c$ value of 1*H*-CAS is estimated to be $\sim$3.5, which suggests that it belongs to the BCS weak-coupling limit.

We have focused our interest on investigating the relationship between the superconducting properties and the electronic states composed of the flat and/or buckling AlSi layers. In this paper, we report the systematic microscopic study of the structure and size of the superconducting gap in a direct manner by tunneling spectroscopy for 6*H*-, 5*H*-, and 1*H*-CAS.

II. EXPERIMENTAL DETAILS

The single crystals of the respective phases (6*H*-, 5*H*-, and 1*H*-CAS) used in the present experiments are identical to those used in our previous studies; thereby, we refer readers to our previous report for the details of the growth conditions and superconducting parameters.[6]

The tunneling spectroscopy measurements were conducted using an *in situ* break-junction technique.[7] The platelike specimen with a size of $3.0\times2.0\times0.5$ mm^3 was cracked

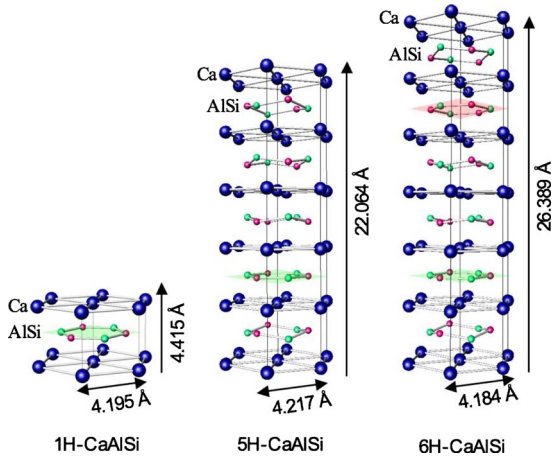

FIG. 1. (Color online) Crystal structure of superstructured specimens (5*H*- and 6*H*-CAS) and 1*H*-CAS. The green and red sheets represent the flat AlSi layer, and their different colors mean a rotation of 60° around the *c* axis. For the space group and detailed structure parameters, see Refs. 5 and 6.

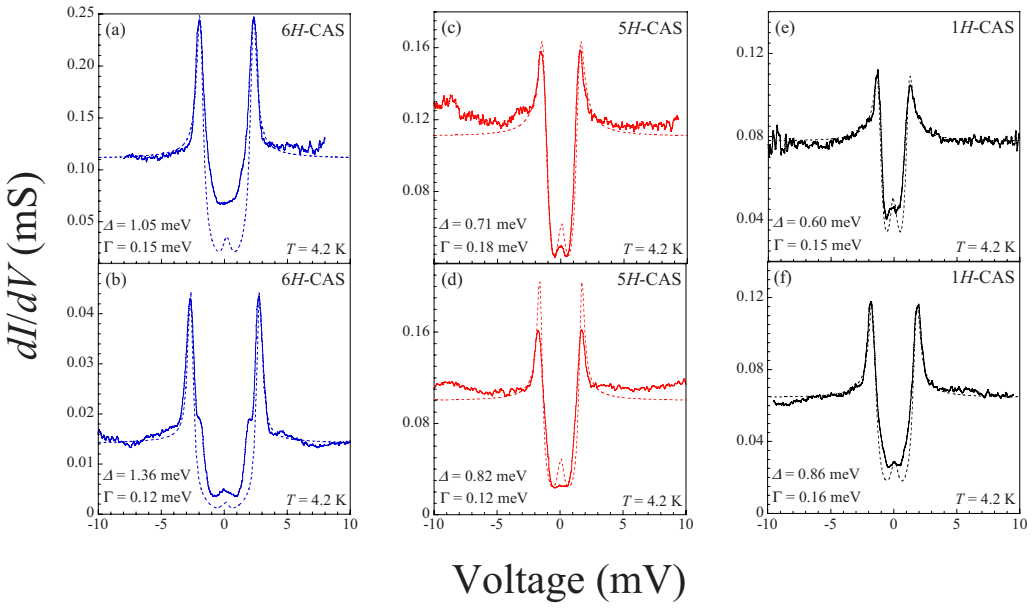

FIG. 2. (Color online) Representative tunneling conductance dI/dV obtained from different break junctions at 4.2 K for 6*H*- [(a) and (b)], 5*H*- [(c) and (d)], and 1*H*-CAS [(e) and (f)]. For the explanation of dashed curves, see the text.

at 4.2 K perpendicular to the length direction just before the measurement, thereby forming a superconductor-insulator-superconductor (SIS) junction with a clean and unaffected interface. This technique enables highly sensitive probing of the structure and size of the superconducting gap (e.g., multigap feature[8]). It is recognized from the SIS junction that the bias voltage between the conductance peaks ($V_{p\text{-}p}$) for tunneling conductance dI/dV corresponds to $4\Delta/e$, where 2Δ is the superconducting gap. The gap size thus obtained at each temperature is just the same as that obtained from conductance fitting using the BCS density of states.[9] Furthermore, with such an SIS junction with an unaffected interface, the gap characteristics can be directly determined, even in the vicinity of T_c, owing to the enhancement of the gap-edge peaks as a result of the piling up of densities of states in both sides of the electrodes.[9] The current (I)-voltage (V) characteristics were measured by the ac modulation technique with a four-probe method.

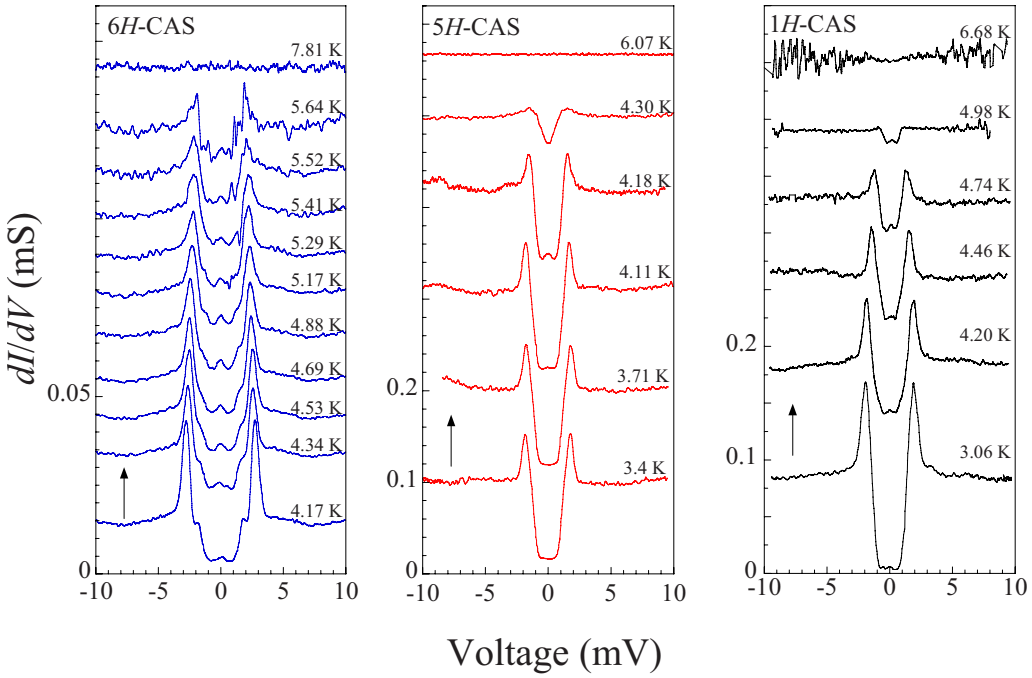

FIG. 3. (Color online) Temperature variations in SIS tunneling conductance for junctions in Figs. 2(b), 2(d), and 2(f) for 6*H*-, 5*H*-, and 1*H*-CAS, respectively.

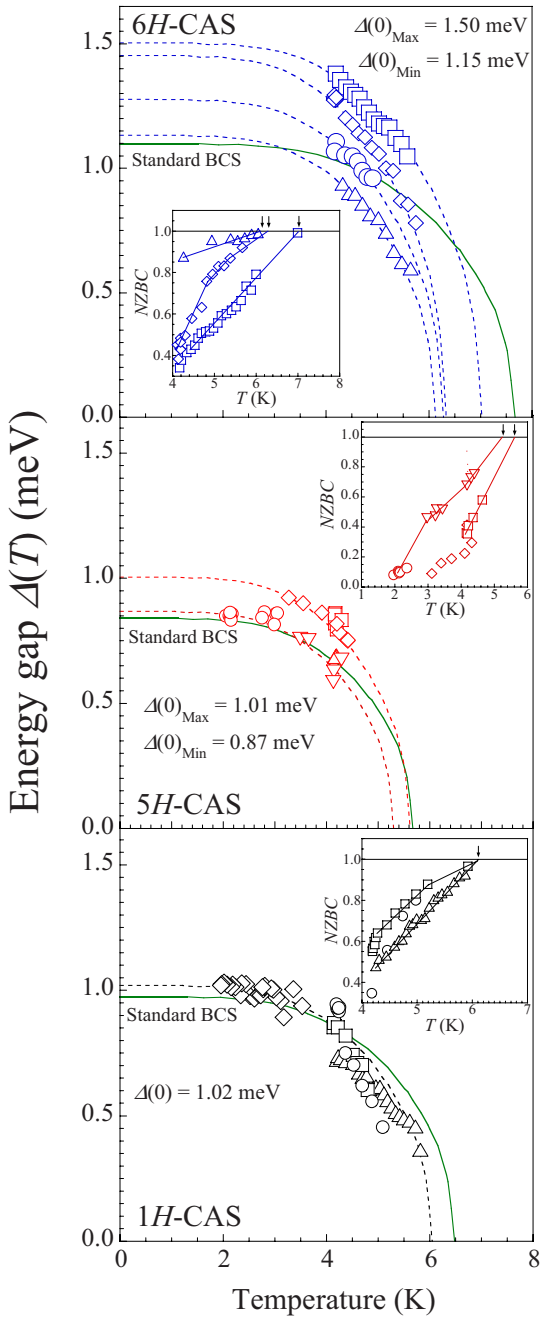

FIG. 4. (Color online) Temperature dependences of energy gaps Δ and normalized zero-bias conductance (NZBC) for 6*H*-, 5*H*-, and 1*H*-CAS. Different symbols in each frame denote different junctions. The solid curves in main panels represent a standard BCS prediction with the respective bulk T_c, while the dashed curves are the scaled BCS curves.

III. EXPERIMENTAL RESULTS AND DISCUSSION

Figure 2 shows the dI/dV spectra obtained from different break junctions at 4.2 K for 6*H*-, 5*H*-, and 1*H*-CAS. We stress that these dI/dV tunneling spectra are highly reproducible and were obtained from several break junctions. As shown in Fig. 2, the sharp gap-edge peaks due to the SIS junction for all specimens were clearly observed. For 6*H*-CAS, the step structure inside the main peaks can be explained by the simultaneous transfer of two particles (*n*-particle tunneling effect) and/or the superconductor-insulator-normal metal tunneling component. The dashed curves in Fig. 2 are calculation results for the tunneling density of states (DOS) $N(E,\Gamma)$ for the SIS junction, assuming the lifetime-broadened BCS DOS proposed by Dynes *et al.*,[10]

$$I(V) = C\int_{-\infty}^{\infty} N(E,\Gamma)N(E+eV,\Gamma)[f(E)-f(E+eV)dE], \tag{1}$$

$$N(E,\Gamma) = |\mathrm{Re}(E-i\Gamma)/\sqrt{(E-i\Gamma)^2-\Delta^2}|, \tag{2}$$

where C is the scaling parameter, Γ is the phenomenological broadening parameter, $f(E)$ is the Fermi distribution function describing the thermal effect, and Δ is the energy gap. For the fitting, we first calculated the tunneling current $I(V)$ using Eqs. (1) and (2) at a fixed temperature with the appropriate parameters Δ and Γ, and then $I(V)$ was numerically differentiated. The agreement between the experimental dI/dV spectra and the calculated ones justifies the assumption that the DOS in CAS is described by the BCS DOS.

Figure 3 shows the temperature variations of SIS tunneling conductance for the junctions in Figs. 2(b), 2(d), and 2(f) for 6*H*-, 5*H*-, and 1*H*-CAS, respectively. The small peak structures at zero bias are due to the Josephson effect and/or thermally excited quasiparticle tunneling effect.[11,12] The gap-edge structures are gradually broadened and suppressed with increasing temperature. We find that the gap structures for all samples completely vanish at T_c.

The temperature dependences of the energy gap Δ and the normalized zero-bias conductance (NZBC $=[dI/dV(0)]/[dI/dV(10\ \mathrm{mV})]$) for 6*H*-, 5*H*-, and 1*H*-CAS are shown in Fig. 4. The different symbols correspond to the different break junctions. The solid curves in the main panels represent the temperature dependence of the standard BCS energy gap having a weak-coupling limit ($2\Delta/k_BT_c=3.52$) for the bulk T_c, while the dashed curves are the scaled BCS curves. Note that multiple fitting curves are needed to reconstruct the temperature dependences of Δ in 5*H*- and 6*H*-CAS. These fitted curves do not cross each other, indicating a systematic behavior of the distributed gaps. The maximum and minimum values of $\Delta(0)$ are listed in Fig. 4, where we can distinguish the range of the ratio $2\Delta/k_BT_c$ among 6*H*-, 5*H*-, and 1*H*-CAS (Table I).

For 5*H*- and 6*H*-CAS, the gap values in the low-temperature limit were extrapolated by fitting the scaled BCS curves, allowing some uncertainties in determining $\Delta(0)$. This procedure is inevitable in deducing the gap data at 0 K. In this case, T_c's of the fitted BCS curves are obtained from the temperature dependence of the zero-bias conductance of each junction, as shown in insets of Fig. 4, from which T_c is precisely determined. We can thus determine a proper range of $\Delta(0)$ that is relatively unscattered and that systematically changes with T_c. On the other hand, we stress that $\Delta(T)$ in

1*H*-CAS can be well fitted by only one component of a scaled BCS curve, indicating a uniform or weakly distributed gap structure.

Here, we discuss the observed difference in the distributions of $\Delta(T)$ for 6*H*-, 5*H*-, and 1*H*-CAS. One of the possible origins of the gap distributions in 5*H*- and 6*H*-CAS is the two-dimensional electronic states, as confirmed by the ratio of inter-/in-plane electrical resistivity, the coherence length,[6] and the magnetic penetration depth.[13] On the other hand, for 1*H*-CAS, a theoretical investigation suggested that the in-plane plasma frequency has almost the same value as the interplane one,[14,15] because of the isotropic effective carrier mass. In fact, the anisotropic Ginzburg-Landau parameter Γ_{GL}, which is related to the ratio of in-/interplane effective carrier mass, for 1*H*-CAS was experimentally estimated to be approximately 1.2, which is considerably smaller than those of 5*H*- and 6*H*-CAS with the superstructure (Γ_{GL} $=3.2-4.0$).[6] Moreover, our recent *ab initio* calculations on the electronic band structures of 5*H*- and 6*H*-CAS indicate that the Fermi surface properties of 5*H*- and 6*H*-CAS are drastically different from those of 1*H*-CAS.[16] In particular, cylindrical Fermi surface sheets appear along the *M*-*L* line in the hexagonal Brillouin zone of 5*H*- and 6*H*-CAS. These results suggest that 5*H*- and 6*H*-CAS possess highly two-dimensional electronic states, which is markedly different from 1*H*-CAS. From this viewpoint, the scattered temperature dependences of the gap in 5*H*- and 6*H*-CAS could be due to the anisotropy of electronic ground states.

We also should mention the possibility that the distribution of $\Delta(T)$ in 5*H*- and 6*H*-CAS is attributable to the spatial modulation in the superconducting order parameter to the proximity effect, and not to the multiple-band superconductivity. This is because each $\Delta(T)$ has different T_c in contrast to the multigap feature exhibiting single T_c. For MgB_2 (Ref. 8) and the layered nitride superconductor,[17] it was reported that the mesoscopic gap distributions and proximity-induced effect could exist owing to inhomogeneous carrier density associated with the layered structures. Hence, such a gap distribution in 5*H*- and 6*H*-CAS cannot be simply connected with the multiple gaped scenario as in MgB_2. Especially, the tunnel conductance for CaAlSi is not described by the correlated two gap model for a two band superconductor, but expressed by a simple BCS model. Moreover, the previous angle-resolved photoemission spectroscopy (ARPES) measurements[18] have suggested that CaAlSi is in sharp contrast to MgB_2 in which multiple gaps are observed.[19] It is notable that CaAlSi exhibits an identical gap magnitude on different Fermi surface sheets around *M* and Γ points in the hexagonal Brillouin zone. Therefore, it is unreasonable that the present tunneling data are evidence of the presence of a multigap structure in this system. It should also be noted that both temperature and magnetic-field dependences of the specific heat show the existence of a BCS gap, thereby showing no evidence for the multiple-gap feature. Consequently, the difference in the distributions of $\Delta(T)$ in 6*H*-, 5*H*-, and 1*H*-CAS probably depends on the dimensionality (two or three dimensional) in the electronic structure involving the proximity effect arising from the layered structure. We note that T_c and the gap value indeed scatter, but their ratio is sufficiently converged to conclude that they are in reasonable agreement with each other.

We next discuss the larger gap ratios observed in 5*H*- and 6*H*-CAS than in 1*H*-CAS. One of the possible origins of the large gap extending to the very strong-coupling regime is associated with the difference in the anisotropic conduction band structures between 6*H*-, 5*H*-, and 1*H*-CAS. The results of ARPES[18] and theoretical investigation[14–16] indicate that the π bands in CAS are mainly composed of $3p_z$ electrons of Al/Si atoms, which possess fully three-dimensional characteristics, while the σ band is derived from the hybridization of $3s$, $3p_x$, and $3p_y$. From the theoretical prediction, the contribution of the π band at the Fermi energy is suppressed with decreasing crystal symmetry, suggesting that the three-dimensionality in the electronic ground states in 5*H*- and 6*H*-CAS is weaker than that in 1*H*-CAS. This leads to the possibility that the conduction band structures are largely modified, including the spectral change in the electron-phonon interaction, thereby resulting in different pairing strengths. The low dimensionality should restrict the electron-phonon interactions, thereby, the interactions with the particular wave vectors could be enhanced to cause the strong-coupling superconductivity, even though T_c is not greatly enhanced possibly because of unavoidable randomness of the real crystal structure.

Finally, it should be noted that the gap sizes for CAS are consistent with those obtained from the previous bulk heat capacity measurements,[6] as listed in Table I. Moreover, such a different gap ratio between superstructured specimens and 1*H*-CAS is further supported by our recent superconducting gap measurements on 6*H*-, 5*H*-, and 1*H*−CaAlSi using high-resolution ARPES.[20] Therefore, we claim that the large gap values observed here in 5*H*- and 6*H*-CAS are due not to surface or local effects but to intrinsic bulk properties. It should be emphasized that a slight T_c increase from 6 to 7.7 K accompanies the drastic enhancement of the ratio

TABLE I. Values of T_c and $2\Delta/k_BT_c$ determined from heat capacity measurements (Ref. 6) and the present tunneling spectroscopy with the break-junction technique.

	Break junction		Heat capacity	
	T_c (K)	$2\Delta/k_BT_c$	T_c (K)	$2\Delta/k_BT_c$
6*H*-CAS	6.1–7.1	4.4–4.9	7.7	5.2
5*H*-CAS	5.3–5.6	3.8–4.2	5.7	4.4
1*H*-CAS	6.1	3.8–3.9	6.5	3.5

$2\Delta/k_BT_c$ from the BCS value of 3.5–3.8 to the extremely strong-coupling one of 4.4–5.0. This is the largest ratio and is comparable to that of MgB_2 with the same crystal structure.[8]

IV. CONCLUSION

We performed tunneling spectroscopy experiments using a break-junction technique on the ternary silicide superconductor CaAlSi with and without a superstructure to elucidate the correlation between the superstructure and the superconducting gap from a microscopic point of view. From the superconducting gap measurements, we found that 6*H*- and 5*H*-CAS belong to a strong-coupling regime, while 1*H*-CAS is a weak-coupling BCS superconductor. These results indicate that the pairing interaction is considerably enhanced by the superstructure formation, which should modify the dimensionality in the electronic ground states and thus the spectral feature of that particular electron-phonon interaction.

ACKNOWLEDGMENTS

This work was partly supported by the 21st COE Program "High-Tech Research Center" Project for Private Universities, a matching fund subsidy from Ministry of Education, Culture, Sports, Science and Technology (MEXT) (2002–2004).

[1] J. Nagamatsu, N. Nakagawa, T. Muranaka, Y. Zenitani, and J. Akimitsu, Nature (London) **410**, 63 (2001).
[2] M. Imai, E. Abe, J. Ye, K. Nishida, T. Kimura, K. Honma, H. Abe, and H. Kitazawa, Phys. Rev. Lett. **87**, 077003 (2001).
[3] M. Imai, K. Nishida, T. Kimura, H. Kitazawa, H. Abe, H. Kito, and K. Yoshii, arXiv:cond-mat/0210692 (unpublished).
[4] M. Imai, El-Hadi S. Sadki, H. Abe, K. Nishida, T. Kimura, T. Sato, K. Hirata, and H. Kitazawa, Phys. Rev. B **68**, 064512 (2003).
[5] H. Sagayama, Y. Wakabayashi, H. Sawa, T. Kamiyama, A. Hoshikawa, S. Harjo, K. Uozato, A. K. Ghosh, M. Tokunaga, and T. Tamegai, J. Phys. Soc. Jpn. **75**, 043713 (2006).
[6] S. Kuroiwa, H. Sagayama, T. Kakiuchi, H. Sawa, Y. Noda, and J. Akimitsu, Phys. Rev. B **74**, 014517 (2006).
[7] T. Ekino, T. Takabatake, H. Tanaka, and H. Fujii, Phys. Rev. Lett. **75**, 4262 (1995).
[8] T. Ekino, T. Takasaki, T. Muranaka, J. Akimitsu, and H. Fujii, Phys. Rev. B **67**, 094504 (2003).
[9] T. Ekino, H. Fujii, M. Kosugi, Y. Zenitani, and J. Akimitsu, Phys. Rev. B **53**, 5640 (1996).
[10] R. C. Dynes, V. Narayanamurti, and J. P. Garno, Phys. Rev. Lett. **41**, 1509 (1978).
[11] J. Bardeen, Phys. Rev. Lett. **6**, 57 (1961).
[12] E. L. Wolf, *Principles of Electron Tunneling Spectroscopy* (Oxford Uninversity Press, New York, 1985).
[13] S. Kuroiwa, K. H. Satoh, A. Koda, R. Kadono, K. Ohishi, W. Higemoto, and J. Akimitsu, J. Phys. Chem. Solids (to be published).
[14] I. I. Mazin and D. A. Papaconstantopoulos, Phys. Rev. B **69**, 180512(R) (2004).
[15] M. Giantomassi, L. Boeri, and G. B. Bachelet, Phys. Rev. B **72**, 224512 (2005).
[16] S. Kuroiwa *et al.* (unpublished).
[17] T. Takasaki, T. Ekino, H. Fujii, and S. Yamanaka, J. Phys. Soc. Jpn. **74**, 2586 (2005).
[18] S. Tsuda, T. Yokoya, S. Shin, M. Imai, and I. Hase, Phys. Rev. B **69**, 100506(R) (2004).
[19] S. Souma, Y. Machida, T. Sato, T. Takahashi, H. Matsui, S.-C. Wang, H. Ding, A. Kaminski, J. C. Campuzano, S. Sasaki, and K. Kadowaki, Nature (London) **423**, 65 (2003).
[20] T. Sato *et al.* (unpublished).